Published in final edited form as:
Methods Mol Biol. 2011 ; 771: 171–187. doi:10.1007/978-1-61779-219-9_9.

Screening of CEST MR Contrast Agents

Xiaolei Song, **Kannie W.Y. Chan**, and **Michael T. McMahon**

Abstract

There has been a tremendous amount of interest in developing new MR contrast agents for cellular and molecular imaging applications such as the visualization of tumors, highlighting areas of angiogenesis, highlighting of contrast agent-labeled therapeutic stem cells, and highlighting of contrast agent-labeled drug delivery vehicles. The contrast properties of paramagnetic and super-paramagnetic relaxation-based agents have allowed MR imaging to be used as a tool for all of the above applications. However, a new class of MR contrast agents, chemical exchange saturation transfer (CEST) agents, provides additional features such as (1) the ability to highlight multiple biological events at once within an image through the distinguishability of the different CEST contrast agents, (2) the ability to toggle the contrast "off-to-on" by applying a saturation pulse, and (3) potentially providing more information about the environment surrounding the contrast agent such as the pH or concentration of metabolites. In this chapter, we will focus on the methods which can be used in terms of acquisition schemes and hardware to screen these agents through MR imaging.

Keywords

MRI; CEST; contrast agents; molecular imaging

1. Introduction

1.1. MR Contrast Agents

Magnetic Resonance Imaging (MRI) is a mature technology which primarily uses the water in tissue of either animals or patients to generate images. This is possible due to the high concentration of water present in tissue, with the overall proton (^{1}H) concentration as high as 110 M. Perturbations in either the concentration or the relaxation properties of the water protons in tissue will produce image contrast, which allows MRI to show excellent soft tissue contrast compared to other imaging modalities. Apart from the endogenous contrast between different imaged soft tissues, the MRI signal intensity can also be perturbed by exogenous materials called MR contrast agents. Through the use of these agents (or probes) the signal in these images, especially where the agents are present, can be altered so that the images are sensitive enough to allow the detection of specific molecular or cellular processes.

To date, there are four major classes of MR molecular probes: (1) paramagnetic agents, such as Gd (1) or Mn (2) complexes or also Mn particles (3) that produce a large positive signal enhancement from decreasing T_1, (2) super-paramagnetic agents, such as iron oxide particles (4), which produce a large negative T_2 contrast. (3) A newer class of probes that has been gaining in popularity are based on nonhydrogen nuclei such as ^{19}F in particles (5–11) or on compounds (12) or drugs (13) or smaller amounts of nuclei using hyperpolarized parahydrogen (14, 15) (*see* **Chapter 11**), hyperpolarized xenon (16–18) (*see* **Chapter 10**), or dynamic nuclear polarization (DNP) (19–23) (*see* **Chapters 11** and **33**). These imaging agents do not interact with water and thus cannot provide anatomical information. Therefore, the images produced by the MR signal from these nuclei are usually co-registered

with the water ^{1}H images to obtain anatomical information. (4) A fourth class, the so-called chemical exchange saturation transfer or CEST agents (24–32), is based on applying a saturation pulse to "switch on" the contrast in water signal through chemical exchange and has now matured with many exciting new features as compared to the other three. This area of research has grown tremendously in the last six years in the number of publications and number of citations of these papers focused on CEST. This review will focus on the unique and interesting properties of CEST contrast agents which have attracted the attention of researchers in this field and the main imaging pulse sequence and acquisition scheme which is now in use to obtain MR images when these contrast agents are present.

1.2. The Basics of CEST Contrast

Magnetic resonance (MR) spectra have been used to study chemical exchange between species for decades, dating back to the first time spectral changes due to exchange were observed in 1951 (33, 34). Chemical exchange processes and their influence on NMR spectra have been presented in many early papers (35–43) in the 1950s and 1960s. One notable study which relates directly to the CEST imaging today was performed by Forsen and Hoffman (37) in which a saturation pulse was placed on resonance with solute protons and then the solvent signal intensity was monitored to study chemical exchange. This experiment, adapted for imaging, is what we call chemical exchange saturation transfer (CEST) but has also been known as magnetization transfer (MT) (*see* **Note 1**). A cartoon depicting the mechanism of this contrast is displayed in Fig. 1.

There are two different categories of chemical exchange which can influence MR spectra: *intramolecular exchange* (for example helix-coil transitions of nucleic acids or the folding/unfolding processes for proteins) and *intermolecular exchange* (for example protonation/deprotonation processes or binding of small molecules to macromolecules). Intermolecular exchange is most relevant for MR contrast agents, as this includes the interactions of a solute molecule (or well-dispersed particle) with the bulk solvent or the source of image signal. In fact, for CEST, we are particularly interested in describing proton exchange with water because MRI is primarily a water imaging technique in the clinic. The reason that CEST is a viable mechanism for contrast in MRI is that the chemical exchange of protons acts as a "saturation amplifier." Low concentrations of CEST agents can be detected due to the many exchanges between their protons and water protons. These exchanges magnify this signal loss as compared to the relative concentration between agent exchangeable protons and water. Robert Balaban and co-workers were the first to demonstrate this amplification and they coined the term CEST to describe this mechanism (24, 25, 27) when they were studying metabolites such as urea, ammonia, and many others. For a more detailed discussion of the mechanism of CEST, we refer the reader to a recent review of this topic (44).

There are a number of MR pulse sequences developed to acquire data on a system in chemical exchange with the resulting NMR spectra used to quantify the exchange time constants. For CEST imaging, however, the main method used is the basic saturation transfer scheme with a saturation pulse incremented across the NMR spectrum and the heights of the peaks observed to determine which spins are exchanging with the others. How does one describe the contrast mechanism for this sequence? The Bloch equations have long been used to describe the trajectory of the magnetization and can be adapted to include terms describing the physical exchange of spins. Assuming a small pool of solute protons (s) and a large pool of water protons (w) while applying B_1 along the x-axis, the Bloch equations for a two-pool proton exchange model are as follows (45):

$$\frac{dM_{xs}}{dt} = -\Delta\omega_s M_{ys} - R_{2s} M_{xs} - k_{sw} M_{xs} + k_{ws} M_{xw} \quad [1]$$

$$\frac{dM_{ys}}{dt} = \Delta\omega_s M_{xs} + \omega_1 M_{zs} - R_{2s} M_{ys} - k_{sw} M_{ys} + k_{ws} M_{yw} \quad [2]$$

$$\frac{dM_{zs}}{dt} = \Delta\omega_1 M_{ys} - R_{1s}(M_{zs} - M_{0s}) - k_{sw} M_{zs} + k_{ws} M_{zw} \quad [3]$$

$$\frac{dM_{xw}}{dt} = -\Delta\omega_w M_{yw} - R_{2w} M_{xw} + k_{sw} M_{xs} - k_{ws} M_{xw} \quad [4]$$

$$\frac{dM_{yw}}{dt} = \Delta\omega_s M_{xw} + \omega_1 M_{zw} - R_{2w} M_{yw} + k_{sw} M_{ys} - k_{ws} M_{yw} \quad [5]$$

$$\frac{dM_{zw}}{dt} = -\Delta\omega_1 M_{yw} - R_{1w}(M_{zw} - M_{0w}) + k_{sw} M_{zs} - k_{ws} M_{zw} \quad [6]$$

in which $\omega_0 = \gamma B_0$ (Larmor frequency of the static magnetic field) and $\omega_1 = \gamma B_1$ (precession frequency to flip the magnetization during an rf pulse); $\Delta\omega_s$ and $\Delta\omega_w$ are the chemical shift differences between the saturation pulse and the solute and water resonance frequencies, respectively; M_0 is the equilibrium magnetization. Proton exchange between the two pools occurs with rates k_{sw} (solute $\rightarrow$ water), and k_{ws} (water $\rightarrow$ solute), and $k_{sw}M_{0s} = k_{ws}M_{0w}$ at equilibrium.

1.3. Types of CEST Agents

For MR imaging using CEST, Balaban and co-workers were the first to come up with the idea of using the saturation transfer experiment for imaging molecules with chemically exchangeable groups (24) and they demonstrated that chemical exchange between protons on metabolites and water could be detected sensitively with MR imaging both ex vivo (25) and in vivo (26) on endogenous metabolites such as urea or ammonia. A cartoon depicting the mechanism for these agents is shown in Fig. 2a. In addition van Zijl and colleagues showed that contrast agents could be constructed based on polymers containing many exchangeable protons such as polypeptides (46) or polynucleic acids (47) with the molar sensitivity of these agents greatly enhanced as compared to the small metabolites. In the so-called amide proton transfer (APT) imaging, Zhou et al. (48, 49) then demonstrated that this CEST effect could in fact be used to image the pH effect in the rat brain during ischemia and also highlight regions with large endogenous protein content, such as is the case in tumors in vivo. In addition and concurrently, Sherry and co-workers as also Aime and co-workers showed that exogenous agents can also be made up of complexes containing paramagnetic lanthanides (50–52) and termed PARACEST agents. These agents have ligated water or other paramagnetically shifted protons that exchange with bulk water. Two cartoons depicting two types of PARACEST agents are shown in Fig. 2b and c. More recently, Terreno and co-workers have shown that liposomes which contain paramagnetic shift agents can be used as CEST agents due to the shifting of the water in the lumen of the liposome compared to the bulk, which they have termed LIPOCEST agents (53, 54). A cartoon depicting this type of agent is shown in Fig. 3a. Other types of CEST-generating particles have been developed by Winter and co-workers (55), and more recently presented by Liu

and co-workers (56), with cartoons depicting the two-exchange behavior of these particles in Fig. 3b and c.

One exception to the case of using protons as CEST agents has been developed by Pines and colleagues using hyperpolarized xenon gas and molecular cages instead of water and CEST agents which are soluble. They have shown that cryptophane cages can be used to create chemical shift differences between free and encapsulated hyperpolarized xenon, with rapid exchange between the two on the timescale of the T_1 (57, 58). This exchange allows saturation transfer imaging of these cages, which they have termed HYPER-CEST. Since hyperpolarization amplifies the available magnetization by $>10^4$, the limitation of imaging xenon as opposed to water protons (used for the other agents and abundant in biological tissues) might be overcome. The set of hardware and methods we discuss in this chapter are not suitable for HYPER-CEST experiments/agents.

2. Materials

2.1. General Requirements

1. A high-field (3 T or above) MR scanner, which can have a medium bore (89 mm) or higher with a relatively homogenous main magnetic field, fast and reliable gradient coils, and a high signal-to-noise radiofrequency (RF) coil.
2. A set of sample containers which fit within the RF coil, typically 1 mm capillary tubes with a holder (typically plastic) to organize the containers within the coil. We have fashioned the holder from 384-well cell culture plates.
3. For our method the most important component is the post-processing to correct the B_0 inhomogeneities present in the CEST images; as such some sort of image processing software is required and can be one of several commercial software packages, including MATLAB (Mathworks, Natick, MA), IDL(ITT visual information solutions, Boulder,CO), or others.
4. The general lab equipment should include a water bath, pH meter, rotary evaporator (rotovap), fluorescence reader (such as the Victor V, PerkinElmer).
5. DIACEST (such as L-arginine, Poly-L-Lysine or others), PARACEST (such as Eu-DOTA-4AmCE or Tm-DOTA-4AmCE) or shift agent (such as Tm-DOTMA) compounds are needed to insert into the liposomes.
6. The components of the liposomes will be required, which includes egg Phosphatidyl Choline (EggPC), cholesterol, 1,2-distearoyl-*sn*-glycero-3-phosphoethanolamine-N-[maleimide(polyethylene glycol) -2000](DSPE-PEG2000) and a fluorescently labeled lipid such as 1,2-dipalmitoyl-*sn*-glycero-3-phosphoethanolamine-N-(lissamine rhodamine B sulfonyl) (RhodPE). These can be purchased from Avanti Polar Lipids.
7. Saline-based buffers are required for dissolving the CEST agents such as 10 mM phosphate-buffered saline (PBS) or 10 mM tris-buffered saline (TBS) or others.
8. Concentrated solutions of NaOH and HCl will be required for titrating the solutions and chloroform will be required for dissolving the liposome components.
9. A 50 mL round bottom flask with a few hollow glass beads are needed to perform the extended hydration of the liposomes.
10. A liposome extruder, (such as a Liposofast-Basic extruder from Avestin) is needed to adjust the size of the liposomes. Also needed are polycarbonate filters (50–400 nm cutoff) which can be purchased from Northern Lipids Inc. Also a dynamic light

scattering instrument such as the ZetaSizer from Malvern Instruments is needed to measure the hydrodynamic size of these nanoparticles.

11. 250 kDa cutoff PVDF dialysis tubing (Spectrum Laboratories, Inc.) and a 2 L beaker are required for separating the liposomes from unencapsulated CEST agent.

2.2. Liposome Sample Influences on CEST Contrast

There are many different ways to prepare DIACEST, PARACEST or LIPOCEST agents. In this chapter, we will describe how to prepare DIACEST liposomes, with the advantage of these being that they can be readily prepared using simple lab equipment, extruded to a variety of sizes (from ∼100 nm to ∼800 nm) and produce sufficient CEST contrast for detecting these particles in vivo. These particles are depicted in Fig. 3b.

1. CEST contrast for these liposomes will vary in part as a function of the permeability of the phospholipid bilayer. This permeability is affected by the lipid/sterol content and also, if cholesterol is added, the relative percentage of cholesterol (mole percentage) to the other components.
2. The surface area–volume (SA–V) ratio of these liposomes also influences the CEST contrast. However the size of the liposome (and resulting SA–V ratio) also affects the biodistribution of the particles so there might not be a choice as to what size liposome should be prepared, even if the maximum contrast is not achieved by this size.

2.3. MRI Pulse Sequences

The following pulse sequences should be available.

1. A multi-slice imaging sequence such as fast spin echo (FSE), or rapid acquisition with relaxation enhancement (RARE) with the ability to place a saturation pulse or pulses in front of the imaging sequence and also with the ability to change the saturation pulse time, field strength, and frequency offset such as that found in the magnetization transfer (MT) module on Bruker scanners.
2. A localized spectroscopy sequence, such as point-resolved Spectroscopy (PRESS).
3. A fast 3D scout image sequence, such as fast low angle shot (FLASH).

2.4. In Vitro B_0 Correction Algorithm

B_0 inhomogeneities, if left uncorrected, can erroneously increase or reduce CEST contrast (59, 60) which presents complications for the practical imaging of these agents. Recently, it was shown that the *z*-spectra produced by incrementing a low-power, short saturation pulse can be used to map the absolute water frequencies of each voxel in an image, an approach termed water saturation shift reference (WASSR) mapping (61). Since the saturation pulse is short and weak, both CEST and conventional magnetization transfer (MT) contributions to the *z*-spectra are minimized and only direct water saturation spectra are obtained. The CEST-weighted images can then be corrected in a pixel-by-pixel manner using the WASSR absolute frequency map and the interpolation. These frequency-weighted images can be used to determine the type of CEST agent contained in each voxel in the image, as shown previously (62, 63).

3. Methods

3.1. Liposome Preparation (see Note 2)

1. Dissolve CEST agent (such as L-arginine (Larg)) in 10 mM phosphate-buffered saline (PBS) (or other buffer such as tris-buffered saline (TBS)) at a concentration of 14 mM and titrate to pH 7.4 using HCl or NaOH.
2. The liposome components will have a molar ratio of eggPC:Chol:DSPE-PEG2000:RhodPE of (46.6:46.6:5:1.8). These are all dissolved in chloroform individually, then transferred to a 50 mL round bottom flask using volumes of 0.47/0.140/0.27/1.0 mL respectively, and then stirred manually in a chemical fume hood.
3. The chloroform is evaporated in a rotovap with the water bath set to 50°C. As a result, the lipids form a thin film that coats the side of the flask.
4. Add a few hollow glass beads and hydrate the lipid thin film with 1 mL of the solution containing dissolved CEST agent. Stir the mixture manually until lipids are no longer visible.
5. Anneal for 2 h in a 55°C water bath and stir occasionally.
6. 20 μL of the solution is put aside for fluorescence measurement of the concentration of the liposomes. The remaining solution that contains liposomes is then extruded to reduce the liposome size using 400, 200, 100, and 50 nm cutoff membranes, using two filters. The liposomes are passed through the 400 nm polycarbonate membranes 21 times first, then depending on the desired liposome size, are passed through the 200 nm and 100 nm membranes also using 21 passes through the filters.
7. After the liposomes are extruded, the unencapsulated agent is removed by dialysis overnight in 1× PBS buffer using 250 kDa cutoff PVDF dialysis tubing (Spectrum Laboratories, Inc.).
8. The size and concentration of the liposomes are measured using dynamic light scattering and fluorescence, respectively.

3.2. General MRI Protocol (see Note 3)

1. The phantom should be centered in both the RF coil of the imaging probe and the magnet bore through adjustment of the position of the imaging probe.
2. The RF coil of the imaging probe is then tuned and matched according to the scanner's ^{1}H Larmor frequency (see your scanner manual for details of this procedure).
3. Next, a scout image is acquired (using for example tripilot RARE, MSME (multi-slice multi-echo), or FLASH on Bruker small animal scanners), with a sufficient field of view (FOV) so that three views from the scout (*XZ*, *YZ*, *XY*) capture the whole phantom.
4. The pulse sequence parameters should be calibrated including resonance frequency offset, pulse power for 90° and 180° flip angles, and receiver gain; and the magnet can be shimmed (although not entirely necessary with the B_0 correction routine we will employ in **Section 3.3**).
5. The desired slice for the CEST experiment should be chosen, based on considerations from the scout image such as the distance to the center of the coil or

position of air bubbles in the sample tubes. Due to the fact that CEST imaging employs a long saturation pulse, a single-slice approach is typically preferred in a CEST acquisition to save time. A single-slice RARE sequence without turning on the saturation pulse is then tested to ensure that the defined single-slice geometry sufficiently covers the region of interest.

3.3. Determining B_0 Inhomogeneity

3.3.1. Shimming—CEST imaging is often (though not always, as demonstrated by Vinogradov and co-workers (64)) a difference imaging technique dependent on the frequency of the solvent and, as such, either good shimming or accurate B_0 maps are crucial to measure CEST contrast. Automatic shimming procedures are available on most scanners (generally restricted to first-order shims), or the shimming can be improved further through manual shimming. The shimming should be performed on a slice with the geometry similar to or equivalent to that used for the CEST imaging and the magnetic field should be shimmed to maximize the signal (*see* **Note 4**).

3.3.2. Estimating B_0 Inhomogeneity Over the CEST Slice—The range of frequencies encompassing the water signal can be determined using the point-resolved spectroscopy (PRESS) sequence without water signal suppression with the voxel geometry approximating the CEST imaging (or up to 50% larger in slice thickness). The typical acquisition parameters used are TR/TE = 2000/20 ms; spectrum acquisition size = 8192; sweep width = 10,080 Hz (25 ppm at 9.4 T); and NA = 1. The full spectral width of the water peak is then used to determine the range of B_0 inhomogeneity, after processing the spectrum (including FFT, baseline correction, apodization, etc.).

3.3.3. WASSR Acquisition—The WASSR images are acquired by adding a saturation pulse (called the magnetization transfer module on Bruker scanners) in front of an FSE or RARE sequence. The saturation pulse we typically use is a 200–500 ms continuous wave (CW) pulse with B_1 = 0.5 μT (21.3 Hz, *see* **Note 5**). The saturation pulse is typically scanned across the entire B_0 inhomogeneity range we determine using PRESS (typically from -1 ppm to +1 ppm with respect to water for twenty 1 mm capillaries in a 20 mm RF coil) using a 0.1 ppm increment between each acquisition. The typical imaging parameters used are acquisition bandwidth = 50 kHz; single slice; 1 mm slice thickness; TE = 6 ms; TR = 1500 ms; RARE factor = 16; FOV = 20 × 20 mm (*see* **Note 6**); and the matrix size is set to 128 frequency-encoding steps and 64 phase-encoding steps. The total acquisition time for generating an absolute B_0 map varies from 3 to 10 min. The error of B_0 estimation is under the hertz level for each pixel at a reasonable signal-to-noise ratio (SNR) (i.e., SNR/pixel > 15), using the parameters listed above.

3.4. High Throughput CEST Imaging

3.4.1. CEST Imaging Parameters—The same saturation transfer (ST) RARE sequences that were used to acquire the WASSR scans can be utilized to acquire CEST images at the relevant saturation frequencies. The typical imaging parameters used are acquisition bandwidth = 50 kHz; single slice; 1 mm slice thickness; TE = 6 ms, TR = 6000 ms; RARE factor = 16; FOV = 20 × 20 mm; 128 × 64 matrix size; 4000 ms CW saturation pulse; B_1 strength = 3.6 μT (153 Hz); and NA = 2. This leads to the acquisition time of approximate 48 s for each image.

3.4.2. High Throughput Collection Scheme—CEST images are collected using a series of CEST-weighted images with the incremented saturation offset to observe the saturation transfer from all the exchangeable protons in the imaging agent, the so-called “z-spectra” approach. For DIACEST liposomes, the frequency can be swept from −5 ppm to +5

ppm in steps of 0.2 ppm. For this sequence of images, the total scan time required will be ~20 min (*see* **Note 7**).

3.5. Image Post-processing and Analysis

3.5.1. Generation WASSR B_0 Maps (see Note 8)

1. The set of WASSR images are used to generate a B_0 map by writing a MATLAB script (or IDL, etc.) to perform the pixelwise fitting (*see* **Section 2.4**) as follows.
2. Pixel by pixel, the vector of MR signal amplitudes, $S_{exp}(x, y)$ are fit for the whole set of WASSR images with the saturation offset vector, $\Delta\omega(x, y)$, using the equation

$$S_{\exp}(x,y)=\left\{\eta^2+\left[\frac{M_0(x,y)}{1+\left(\frac{\omega_1(x,y)}{\Delta\omega(x,y)-\delta\omega_0(x,y)}\right)^2\frac{T_1(x,y)}{T_2(x,y)}}\right]^2\right\}^{1/2}$$

to estimate $\delta\omega_0(x, y)$. The non-linear fitting function (*lsqcurvefit*) in MATLAB can be used to perform this fitting, with M_0, $\delta\omega_0$, and $\left(\frac{T_1}{T_2}\omega_1^2\right)$ as floating parameters. The experimental noise (η) is estimated from the mean signal of a noise-only region of the image (the air region between the capillaries) and is then fixed.

3. The absolute B_0 map is constructed as a result of the fits from Step 2 above, by collecting the fit $\delta\omega_0(x, y)$ for each pixel and plotting this, thus providing the water shift information needed to correct the B_0 in the CEST images. The resulting map will look as shown in Fig. 4a.

3.5.2. Processing Raw CEST Data

1. The saturation offsets of the CEST images are corrected pixel-by-pixel using the WASSR B_0 map and the expression $\Delta\omega(x, y)_{corrected} = \Delta\omega(x, y) - \Delta\omega_0(x, y)$. In order to perform this correction, the original set of CEST images are interpolated pixelwise to obtain the water signal amplitude, $S_{x,y}(\Delta\omega_{interp})$, at the desired offsets using the cubic-spline fitting (*spline*) function in MATLAB. An example of the resulting MTR_{asym} map for such a phantom is shown in Fig. 4c at the shift of the exchangeable guanidyl protons (1.8 ppm).
2. The CEST *z*-spectrum can then be plotted using the scaled signal intensity, $S^{\Delta\omega}/S_0$ as a function of saturation offset frequency with respect to water. Typically, region of interest (ROI) masks are manually drawn over each tube in the phantom (one way is to use ROI Draw in Matlab) and the mean intensities of the selected tubes are used to plot the *z*-spectra. Examples of *z*-spectra correction are shown in Fig. 4d for L-arginine and Fig. 4e for 2% agar (which should display no CEST contrast).
3. The CEST contrast is quantified for each tube by calculating the asymmetry in the magnetization transfer ratio (MTR_{asym}), as defined by $MTR_{asym} = (S^{-\Delta\omega} - S^{\Delta\omega})/S^{-\Delta\omega}$. The MTR_{asym} for each pixel should be calculated and used to construct the parametric map, MTR_{asym} map, which represents the distribution of CEST contrast. An example of the resulting MTR_{asym} map for such a phantom is shown in Fig. 4c at the shift of the exchangeable guanidyl protons (1.8 ppm). For a good CEST liposome, the CEST contrast is often in the range of 30% or higher.

4. Note

1. Magnetization transfer (MT) is more commonly used in the context of signal transfer between immobilized protons and water—in contrast to the transfer of magnetization from exchangeable protons on a CEST agent which possess a sharp resonance line due to the tumbling of the agent.
2. This procedure is modified from the extended hydration method (65) using egg phosphatidyl choline (EggPC), cholesterol (Chol), distearoyl-phosphatidyl-ethanolamine conjugated to polyethylene glycol (molecular weight = 2000 D, DSPE-PEG2000) and rhodamine (Rh)-labeled phosphatidyl-ethanolamine purchased from Avanti Polar Lipids.
3. The MR collection and processing is similar to that described in **Chapter 36**, without the need of equipment for animal anesthesia.
4. For manual shimming, the procedure must be performed in an iterative manner since the shimming coils are coupled to each other and affect all three dimensions (*see also* the handbook of your scanner).
5. For converting tesla to hertz, the equation $f = \gamma B_0$ should be used in which γ is the gyromagnetic ratio and is 42.57 MHz/T for ^{1}H protons.
6. The FOV is determined by the RF coil size and amount of sample tubes enclosed in the phantom. If long capillaries are used, the slice thickness can be increased substantially to improve the SNR.
7. When using a clinical imager, the automated shimming and frequency adjustments must be turned off between the consecutive WASSR-CEST images. This is not an issue for high-resolution spectrometers, where these are not automatically adjusted before each scan.
8. In order to reduce the post-processing time, voxels which contain only noise in the MRI images can be removed through thresholding, for example, requiring $SNR \geq 15$.

References

1. Caravan P, Ellison JJ, McMurry TJ, Lauffer RB. Gadolinium(III) chelates as MRI contrast agents: structure, dynamics, and applications. Chemical Reviews. 1999; 99:2293–2352. [PubMed: 11749483]
2. Rocklage SM, Cacheris WP, Quay SC, Hahn FE, Raymond KN. Synthesis and characterization of a paramagnetic chelate for magnetic resonance imaging enhancement. Inorgnic Chemistry. 1989; 28:477–485.
3. Na HB, Lee JH, An K, Park YI, Park M, Lee IS, Nam DH, Kim ST, Kim SH, Kim SW, Lim KH, Kim KS, Kim SO, Hyeon T. Development of a T_1 contrast agent for magnetic resonance imaging using MnO nanoparticles. Angewandte Chemie International Edition England. 2007; 46:5397–5401.
4. Bjornerud A, Johansson L. The utility of superparamagnetic contrast agents in MRI: theoretical consideration and applications in the cardiovascular system. NMR in Biomedicine. 2004; 17:465–77. [PubMed: 15526351]
5. Srinivas M, Morel PA, Ernst LA, Laidlaw DH, Ahrens ET. Fluorine-19 MRI for visualization and quantification of cell migration in a diabetes model. Magnetic Resonance in Medicine. 2007; 58:725–734. [PubMed: 17899609]
6. Janjic JM, Srinivas M, Kadayakkara DKK, Ahrens ET. Self-delivering nanoemulsions for dual fluorine-19 MRI and fluorescence detection. Journal of the American Chemical Society. 2008; 130:2832–2841. [PubMed: 18266363]

7. Waters EA, Chen JJ, Yang XX, Zhang HY, Neumann R, Santeford A, Arbeit J, Lanza GM, Wickline SA. Detection of targeted perfluorocarbon nanoparticle binding using F-19 diffusion weighted MR spectroscopy. Magnetic Resonance in Medicine. 2008; 60:1232–1236. [PubMed: 18956417]
8. Waters EA, Chen JJ, Allen JS, Zhang HY, Lanza GM, Wickline SA. Detection and quantification of angiogenesis in experimental valve disease with integrin-targeted nanoparticles and 19-fluorine MRI/MRS. Journal of Cardiovascular Magnetic Resonance. 2008; 10:43. [PubMed: 18817557]
9. Ruiz-Cabello J, Walczak P, Kedziorek DA, Chacko VP, Schmieder AH, Wickline SA, Lanza GM, Bulte JWM. In vivo “hot spot” MR imaging of neural stem cells using fluorinated nanoparticles. Magnetic Resonance in Medicine. 2008; 60:1506–1511. [PubMed: 19025893]
10. Partlow KC, Chen JJ, Brant JA, Neubauer AM, Meyerrose TE, Creer MH, Nolta JA, Caruthers SD, Lanza GM, Wickline SA. F-19 magnetic resonance imaging for stem/progenitor cell tracking with multiple unique perfluorocarbon nanobeacons. FASEB Journal. 2007; 21:1647–1654. [PubMed: 17284484]
11. Neubauer AM, Caruthers SD, Hockett FD, Cyrus T, Robertson JD, Allen JS, Williams TD, Fuhrhop RW, Lanza GM, Wickline SA. Fluorine cardiovascular magnetic resonance angiography in vivo at 1.5 T with perfluorocarbon nanoparticle contrast agents. Journal of Cardiovascular Magnetic Resonance. 2007; 9:565–573. [PubMed: 17365236]
12. Hunjan S, Mason RP, Constantinescu A, Peschke P, Hahn EW, Antich PP. Regional tumor oximetry: F-19 NMR spectroscopy of hexafluorobenzene. International Journal of Radiation Oncology, Biology, Physics. 1998; 41:161–171.
13. Yu JX, Kodibagkar VD, Cui WN, Mason RP. F-19: a versatile reporter for non-invasive physiology and pharmacology using magnetic resonance. Current Medicinal Chemistry. 2005; 12:819–848. [PubMed: 15853714]
14. Adams RW, Aguilar JA, Atkinson KD, Cowley MJ, Elliott PIP, Duckett SB, Green GGR, Khazal IG, Lopez-Serrano J, Williamson DC. Reversible interactions with para-hydrogen enhance NMR sensitivity by polarization transfer. Science. 2009; 323:1708–1711. [PubMed: 19325111]
15. Bouchard LS, Burt SR, Anwar MS, Kovtunov KV, Koptyug IV, Pines A. NMR imaging of catalytic hydrogenation in microreactors with the use of para-hydrogen. Science. 2008; 319:442–445. [PubMed: 18218891]
16. Navon G, Song YQ, Room T, Appelt S, Taylor RE, Pines A. Enhancement of solution NMR and MRI with laser-polarized xenon. Science. 1996; 271:1848–1851.
17. Goodson BM, Song YQ, Taylor RE, Schepkin VD, Brennan KM, Chingas GC, Budinger TF, Navon G, Pines A. In vivo NMR and MRI using injection delivery of laser-polarized xenon. Proceedings of the National Academy of Sciences of the United States of America. 1997; 94:14725–14729. [PubMed: 9405680]
18. Song YQ, Gaede HC, Pietrass T, Barrall GA, Chingas GC, Ayers MR, Pines A. Spin-polarized Xe-129 gas imaging of materials. Journal of Magnetic Resonance Series A. 1995; 115:127–130.
19. Ardenkjaer-Larsen JH, Fridlund B, Gram A, Hansson G, Hansson L, Lerche MH, Servin R, Thaning M, Golman K. Increase in signal-to-noise ratio of > 10,000 times in liquid-state NMR. Proceedings of the National Academy of Sciences of the United States of America. 2003; 100:10158–10163. [PubMed: 12930897]
20. Golman K, Ardenaer-Larsen JH, Petersson JS, Mansson S, Leunbach I. Molecular imaging with endogenous substances. Proceedings of the National Academy of Sciences of the United States of America. 2003; 100:10435–10439. [PubMed: 12930896]
21. Day SE, Kettunen MI, Gallagher FA, Hu DE, Lerche M, Wolber J, Golman K, Ardenkjaer-Larsen JH, Brindle KM. Detecting tumor response to treatment using hyperpolarized C-13 magnetic resonance imaging and spectroscopy. Nature Medicine. 2007; 13:1382–1387.
22. Golman K, in't Zandt R, Lerche M, Pehrson R, Ardenkjaer-Larsen JH. Metabolic imaging by hyperpolarized C-13 magnetic resonance imaging for in vivo tumor diagnosis. Cancer Research. 2006; 66:10855–10860. [PubMed: 17108122]
23. Gallagher FA, Kettunen MI, Day SE, Hu DE, Ardenkjaer-Larsen JH, in't Zandt R, Jensen PR, Karlsson M, Golman K, Lerche MH, Brindle KM. Magnetic resonance imaging of pH in vivo

using hyperpolarized C-13-labelled bicarbonate. Nature. 2008; 453:940–U73. [PubMed: 18509335]

24. Wolff SD, Balaban RS. NMR imaging of labile proton-exchange. Journal of Magnetic Resonance. 1990; 86:164–169.
25. Guivel-Scharen V, Sinnwell T, Wolff SD, Balaban RS. Detection of proton chemical exchange between metabolites and water in biological tissues. Journal of Magnetic Resonance. 1998; 133:36–45. [PubMed: 9654466]
26. Dagher AP, Aletras A, Choyke P, Balaban RS. Imaging of urea using chemical exchange-dependent saturation transfer at 1.5 T. Journal of Magnetic Resonance Imaging. 2000; 12:745–748. [PubMed: 11050645]
27. Ward KM, Aletras AH, Balaban RS. A new class of contrast agents for MRI based on proton chemical exchange dependent saturation transfer (CEST). Journal of Magnetic Resonance. 2000; 143:79–87. [PubMed: 10698648]
28. Ward KM, Balaban RS. Determination of pH using water protons and chemical exchange dependent saturation transfer (CEST). Magnetic Resonance in Medicine. 2000; 44:799–802. [PubMed: 11064415]
29. Aime S, Crich SG, Gianolio E, Giovenzana GB, Tei L, Terreno E. High sensitivity lanthanide(III) based probes for MR-medical imaging. Coordination Chemistry Reviews. 2006; 250:1562–1579.
30. Sherry AD, Woods M. Chemical exchange saturation transfer contrast agents for magnetic resonance imaging. Annual Review of Biomedical Engineering. 2008; 10:391–411.
31. Zhou J, van Zijl PCM. Chemical exchange saturation transfer imaging and spectroscopy. Progress in NMR Spectroscopy. 2006; 48:109–136.
32. Yoo B, Pagel MD. An overview of responsive MRI contrast agents for molecular imaging. Frontiers in Bioscience. 2008; 13:1733–1752. [PubMed: 17981664]
33. Liddel U, Ramsey NF. Temperature dependent magnetic shielding in ethyl alcohol. Journal of Chemical Physics. 1951; 19:1608.
34. Arnold JT, Packard ME. Variations in absolute chemical shift of nuclear induction signals of hydroxyl groups of methyl and ethyl alcohol. Journal of Chemical Physics. 1951; 19:1608–1609.
35. Gutowsky HS, Holm CH. Rate processes and nuclear magnetic resonance spectra.2. hindered internal rotation of amides. Journal of Chemical Physics. 1956; 25:1228–1234.
36. Gutowsky HS, Saika A. Dissociation, chemical exchange, and the proton magnetic resonance in some aqueous electrolytes. Journal of Chemical Physics. 1953; 21:1688–1694.
37. Forsen S, Hoffman RA. Study of moderately rapid chemical exchange reactions by means of nuclear magnetic double resonance. Journal of Chemical Physics. 1963; 39:2892–2901.
38. McConnell HM. Reaction rates by nuclear magnetic resonance. Journal of Chemical Physics. 1958; 28:430–431.
39. Arnold DL. Magnetic resonances of protons in ethyl alcohol. Physical Review. 1956; 102:135–150.
40. Allerhand A, Gutowsky HS. Spin-echo NMR studies of chemical exchange. 1. some general aspects. Journal of Chemical Physics. 1964; 41:2115–2126.
41. Gutowsky HS, Vold RL, Wells EJ. Theory of chemical exchange effects in magnetic resonance. Journal of Chemical Physics. 1965; 43:4107.
42. Woessner DE. Nuclear transfer effects in nuclear magnetic resonance pulse experiments. Journal of Chemical Physics. 1961; 35:41–48.
43. McConnell HM, Thompson DD. Molecular transfer of nonequilibrium nuclear spin magnetization. Journal of Chemical Physics. 1957; 26:958–959.
44. Zhou JY, van Zijl PCM. Chemical exchange saturation transfer imaging and spectroscopy. Progress in Nuclear Magnetic Resonance Spectroscopy. 2006; 48:109–136.
45. Zhou J, Wilson DA, Sun PZ, Klaus JA, van Zijl PCM. Quantitative description of proton exchange processes between water and endogenous and exogenous agents for WEX, CEST, and APT experiments. Magnetic Resonance in Medicine. 2004; 51:945–952. [PubMed: 15122676]

46. Goffeney N, Bulte JWM, Duyn J, Bryant LH, van Zijl PCM. Sensitive NMR detection of cationic-polymer-based gene delivery systems using saturation transfer via proton exchange. Journal of the American Chemical Society. 2001; 123:8628–8629. [PubMed: 11525684]
47. Snoussi K, Bulte JWM, Gueron M, van Zijl PCM. Sensitive CEST agents based on nucleic acid imino proton exchange: detection of poly(rU) and of a dendrimer-poly(rU) model for nucleic acid delivery and pharmacology. Magnetic Resonance in Medicine. 2003; 49:998–1005. [PubMed: 12768576]
48. Zhou J, Lal B, Wilson DA, Laterra J, van Zijl PC. Amide proton transfer (APT) contrast for imaging of brain tumors. Magnetic Resonance in Medicine. 2003; 50:1120–1126. [PubMed: 14648559]
49. Zhou J, Payen JF, Wilson DA, Traystman RJ, van Zijl PC. Using the amide proton signals of intracellular proteins and peptides to detect pH effects in MRI. Nature Medicine. 2003; 9:1085–1090.
50. Zhang S, Merritt M, Woessner DE, Lenkinski RE, Sherry AD. PARACEST agents: modulating MRI contrast via water proton exchange. Accounts of Chemical Research. 2003; 36:783–790. [PubMed: 14567712]
51. Aime S, Delli Castelli D, Terreno E. Novel pH-reporter MRI contrast agents. Angewandte Chemie-International Edition. 2002; 41:4334–4336.
52. Zhang S, Winter P, Wu K, Sherry AD. A novel europium(III)-based MRI contrast agent. Journal of the American Chemical Society. 2001; 123:1517–1518. [PubMed: 11456734]
53. Aime S, Castelli DD, Terreno E. Highly sensitive MRI chemical exchange saturation transfer agents using liposomes. Angewandte Chemie-International Edition. 2005; 44:5513–5515.
54. Terreno E, Cabella C, Carrera C, Castelli DD, Mazzon R, Rollet S, Stancanello J, Visigalli M, Aime S. From spherical to osmotically shrunken paramagnetic liposomes: an improved generation of LIPOCEST MRI agents with highly shifted water protons. Angewandte Chemie-International Edition. 2007; 46:966–968.
55. Winter PM, Cai K, Chen J, Adair CR, Kiefer GE, Athey PS, Gaffney PJ, Buff CE, Robertson JD, Caruthers SD, Wickline SA, Lanza GM. Targeted PARACEST nanoparticle contrast agent for the detection of fibrin. Magnetic Resonance in Medicine. 2006; 56:1384–1388. [PubMed: 17089356]
56. Liu, G.; Har-el, YE.; Moake, M.; Long, C.; Walczak, P.; Gilad, AA.; Zhang, J.; Cardona, A.; Jamil, M.; Sgouros, G.; Bulte, JWM.; van Zijl, PCM.; McMahon, MT. Proceedings of ISMRM. Stockholm, SWE: 2010. In vivo imaging of lymphatic delivery of multi-color DIACEST liposomes.
57. Schröder L, Lowery TJ, Hilty C, Wemmer DE, Pines A. Molecular imaging using a targeted magnetic resonance hyperpolarized biosensor. Science. 2006; 314:446–449. [PubMed: 17053143]
58. Schröder L, Meldrum T, Smith M, Lowery TJ, Wemmer DE, Pines A. Temperature response of Xe-129 depolarization transfer and its application for ultrasensitive NMR detection. Physical Review Letters. 2008; 100:257603. [PubMed: 18643704]
59. Stancanello J, Terreno E, Castelli DD, Cabella C, Uggeri F, Aime S. Development and validation of a smoothing-splines-based correction method for improving the analysis of CEST-MR images. Contrast Media & Molecular Imaging. 2008; 3:136–149. [PubMed: 18683280]
60. Sun PZ, Farrar CT, Sorensen AG. Correction for artifacts induced by *B*-0 and *B*-1 field inhomogeneities in pH-Sensitive chemical exchange saturation transfer (CEST) Imaging. Magnetic Resonance in Medicine. 2007; 58:1207–1215. [PubMed: 17969015]
61. Kim M, Gillen J, Landman BA, Zhou J, van Zijl PCM. WAter Saturation Shift Referencing (WASSR) for chemical exchange saturation transfer experiments. Magnetic Resonance in Medicine. 2009; 61:1441–1450. [PubMed: 19358232]
62. McMahon MT, Gilad AA, DeLiso MA, Berman SM, Bulte JW, van Zijl PC. New “multicolor” polypeptide diamagnetic chemical exchange saturation transfer (DIACEST) contrast agents for MRI. Magnetic Resonance in Medicine. 2008; 60:803–812. [PubMed: 18816830]
63. Aime S, Carrera C, Delli Castelli D, Geninatti Crich S, Terreno E. Tunable imaging of cells labeled with MRI-PARACEST agents. Angewandte Chemie-International Edition England. 2005; 44:1813–1815.

64. Vinogradov E, Zhang S, Lubag A, Balschi JA, Sherry AD, Lenkinski RE. On-resonance low *B*1 pulses for imaging of the effects of PARACEST agents. Journal of Magnetic Resonance. 2005; 176:54–63. [PubMed: 15979362]

65. Castile JD, Taylor KM. Factors affecting the size distribution of liposomes produced by freeze–thaw extrusion. International Journal of Pharmaceutics. 1999; 188:87–95. [PubMed: 10528086]

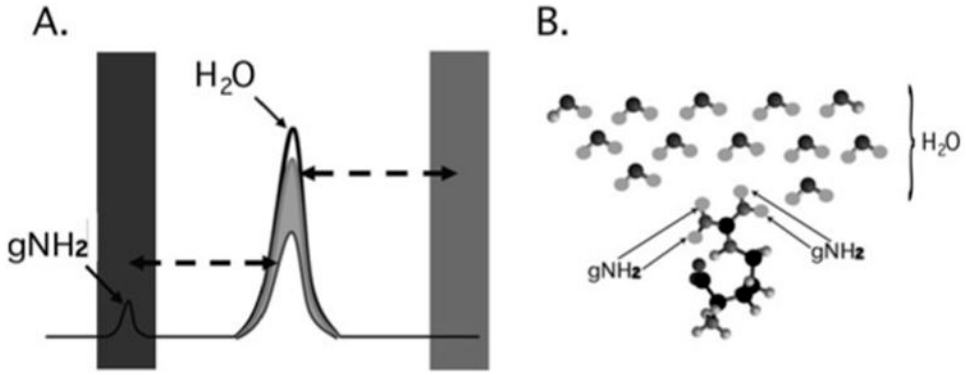

Fig. 1.

Cartoon depicting the mechanism of CEST contrast for L-arginine dissolved in water. (**a**) Saturation pulses are placed either on resonance with the exchangeable guanidyl protons or off resonance and on the opposite side of the water resonance. The CEST contrast (MTR_{asym}) is the difference between the two experiments. (**b**) L-arginine dissolved in water. The guanidyl protons exchange rapidly such that the guanidyl proton saturation spreads through the network of solvent water protons.

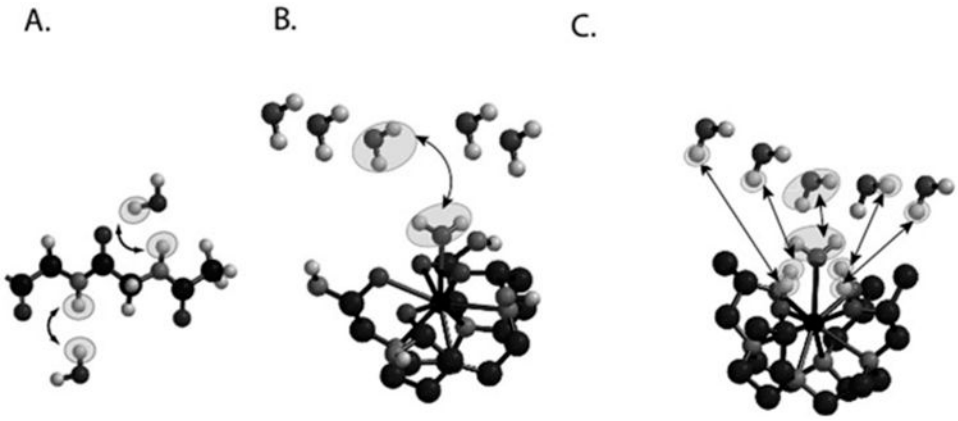

Fig. 2.

Cartoon demonstrating the three different types of CEST contrast agents. (**a**) DIACEST N-acetyl-Gly-Gly fragment with chemical exchange occurring between the backbone NH protons and water. (**b**) PARACEST Ln(DOTAm) fragment with chemical exchange occurring between ligated and free water. (**c**) PARACEST Ln (with chemical exchange occurring between ligated and free water and also between ligated alcohol protons and water.

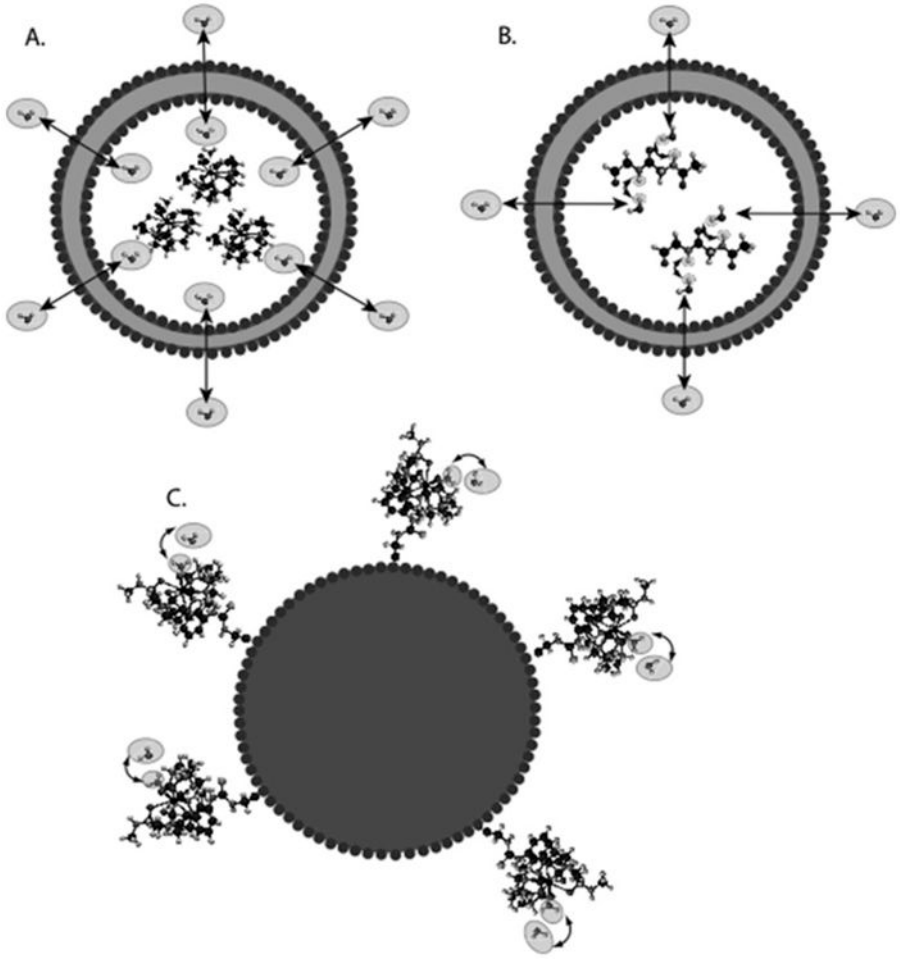

Fig. 3.

Diagram of the contrast mechanism for three different types of CEST contrast particles. (**a**) Traditional LIPOCEST agents, with shift agent enclosed in the liposomal lumen, and chemical exchange occurring between the interior and exterior water. (**b**) Two-hop LIPOCEST agents, with CEST agent (not shift agent) enclosed in the liposomal lumen, and proton exchange occurring between agent and interior water, then interior water and exterior water. (**c**) CEST coated particles, where the exchange occurs entirely on the periphery of the particle.

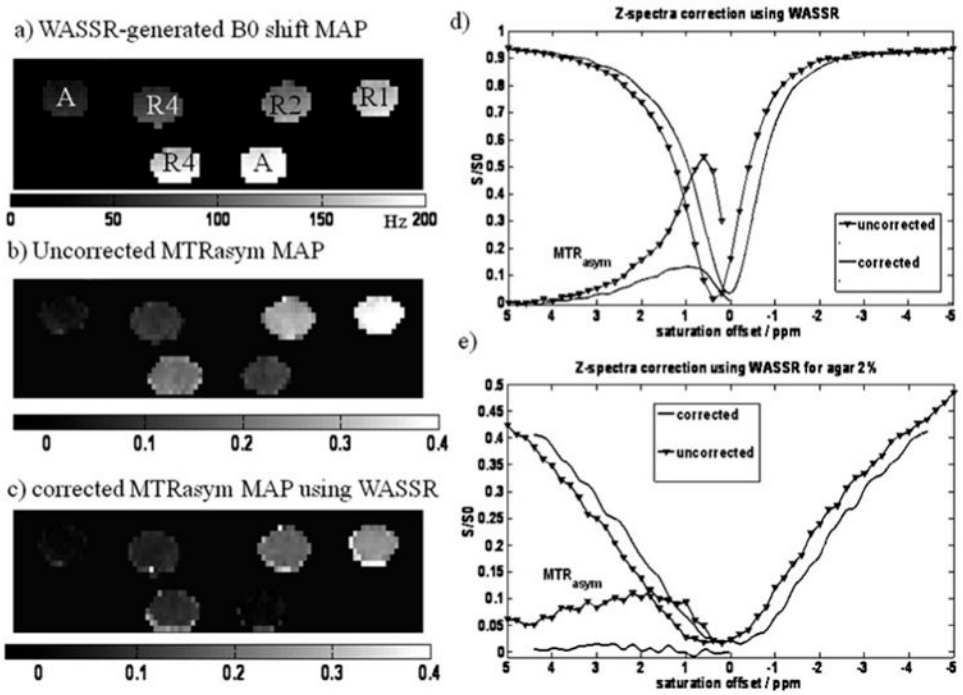

Fig. 4.

An example of B_0 correction of CEST images. (**a**) B_0 map derived from WASSR image set with the sample configuration. A: agar 2%, R1, R2, R4 represent 10 mM, 5 mM, 2.5 mM L-arginine in PBS respectively (the B_0 shift is displayed for this phantom from 0 to 200 Hz from the carrier frequency). (**b**) Uncorrected MTR_{asym} map at 1.8 ppm (MTR_{asym} is displayed on a scale from 0 to 0.4) and (**c**) corrected MTR_{asym} map using as described in **Section 3.5.2** (MTR_{asym} is displayed on a scale from 0 to 0.4). (**d**) Uncorrected and corrected *z*-spectra and MTR_{asym} curves for the lower R4 sample shown in **a**–**c**. (**e**) Uncorrected and corrected *z*-spectra and MTR_{asym} curves for the lower agar sample.